PREPARED FOR THE U.S. DEPARTMENT OF ENERGY,
UNDER CONTRACT DE-AC02-76-CHO-3073

PPPL-2646
UC-420

PPPL-2646

# TEMPORAL BEHAVIOR OF NEUTRAL PARTICLE FLUXES IN TFTR NEUTRAL BEAM INJECTORS

BY

J.H. KAMPERSCHROER, G.M. GAMMEL, A.L. ROQUEMORE,
L.R. GRISHAM, H.W. KUGEL, S.S. MEDLEY, T.E. O'CONNOR,
T.N. STEVENSON, A. VON HALLE, AND M.D. WILLIAMS

September 1989

PRINCETON
PLASMA PHYSICS
LABORATORY

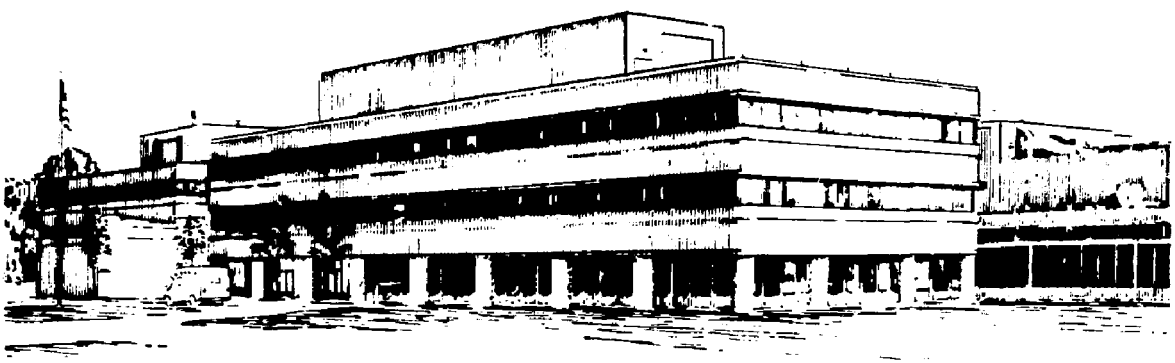

PRINCETON UNIVERSITY, PRINCETON, NEW JERSEY

NOTICE

Available from:

National Technical Information Service
U.S. Department of Commerce
5285 Port Royal Road
Springfield, Virginia 22161
703-487-4650

Use the following price codes when ordering:

Price: Printed Copy A03
Microfiche A01

PPPL--2646

DE90 000850

# Temporal Behavior of Neutral Particle Fluxes in TFTR Neutral Beam Injectors

J. H. Kamperschroer, G. M. Gammel, A. L. Roquemore, L. R. Grisham, H. W. Kugel, S. S. Medley, T. E. O'Connor, T. N. Stevenson, A. von Halle, and M. D. Williams

*Princeton Plasma Physics Laboratory, Princeton University, PO Box 451, Princeton, NJ 08543*

## ABSTRACT

Data from an E ⨯ B charge exchange neutral analyzer (CENA), which views down the axis of a neutral beamline through an aperture in the target chamber calorimeter of the TFTR neutral beam test facility, exhibit two curious effects. First, there is a turn-on transient lasting tens of milliseconds having a magnitude up to three times that of the steady-state level. Second, there is a 720 Hz, up to 20% peak-to-peak, fluctuation persisting the entire pulse duration. The turn-on transient occurs as the neutralizer/ion source system reaches a new pressure equilibrium following the effective ion source gas throughput reduction by particle removal as ion beam. Widths of the transient are a function of the gas throughput into the ion source, decreasing as the gas supply rate is reduced. Heating of the neutralizer gas by the beam is assumed responsible, with gas temperature increasing as gas supply rate is decreased. At low gas supply rates, the transient is primarily due to dynamic changes in the neutralizer line density and/or beam species composition. Light emission from the drift duct corroborate the CENA data. At high gas supply rates, dynamic changes in component divergence and/or spatial profiles of the source plasma are necessary to explain the observations. The 720 Hz fluctuation is attributed to a 3% peak-to-peak ripple of 720 Hz on the arc power supply amplified by the quadratic relationship between beam divergence and beam current. Tight collimation by CENA apertures cause it to accept a very small part of the ion source's velocity space, producing a signal linearly proportional to beam divergence. Estimated fluctuations in the peak power density delivered to the plasma under these conditions are a modest 3-8% peak to peak. The effects of both phenomena on the injected neutral beam can be ameliorated by careful operation of the ion sources.

## INTRODUCTION

Previous results obtained on the Tokamak Fusion Test Reactor (TFTR) neutral beams indicated a neutralization efficiency significantly below that predicted by room temperature gas dynamics in the neutralizer.[1] This anomalous neutralization, first observed on test facilities at Fontenay-aux-Roses[2,3] and at the Joint European Torus (JET),[4] was explained as beam heating of the neutralizer gas.[5] Not all neutral beam laboratories with similar injectors and ion sources have, however, observed this phenomenon.[6]

Data relevant to the study of the neutralizer line density have been obtained from an E ∥ B charge exchange neutral analyzer (CENA)[7] used on the TFTR neutral beam test facility.[8] The analyzer viewed the ion source along the beam axis, through a 2.5 cm aperture located in the target chamber calorimeter. Momentum and mass analysis of the particles provided simultaneous time-resolved detection of all three neutral components (full-, half-, and third-energy) of the beam. Variations in neutralizer line density affect the ion to neutral conversion efficiency and induce amplitude changes in the CENA signals, allowing the beam to serve as a probe of the neutralizer gas.

A series of beam pulses were examined over which significant changes were made in the rate at which gas was delivered to the ion source. At the lower gas flow rates, anomalously low neutral fractions were measured. Neutralizer gas heating is assumed responsible. Data from the CENA revealed two curious effects. First, there was generally a sizeable turn-on transient, persisting for tens of milliseconds, on the signals of the full- and third-energy components, but not on the half-energy component. At the lowest gas flow rates studied, the peak of the turn-on transient was three times higher than that of the following steady-state plateau. Second, all components exhibit 10-15% peak-to-peak fluctuations, with a frequency of 720 Hz, for the duration of the pulse.

A computer program, developed to study TFTR vacuum vessel pump-down transients,[9] was utilized to model neutralizer gas dynamics. The behavior of the neutralizer gas line density during the turn-on transient was modelled with the assumption of room temperature gas. Conductances were calculated based upon molecular, transition, and viscous flow formulae depending upon the local pressure at each time and spatial point.

# I. EXPERIMENTAL APPARATUS

## A. TFTR Neutral Beam Test Facility

A neutral beam test facility was constructed at the Princeton Plasma Physics Laboratory (PPPL) to integrate and diagnose the neutral beamline, power system, and ion source. Figures 1 and 2 are schematic plan and elevation views, respectively, of this facility which consisted of a target chamber, containing a calorimeter at a location simulating that of the plasma, connected to a beamline by a drift duct. The beamline was identical in most respects to those in use on TFTR, with the exception that it possessed enhanced diagnostic capability. The CENA was attached to the rear of the target chamber, viewing upstream toward the ion source.

Of the three ion source positions indicated in Fig. 1, only the central one was used in the test facility. An ion beam originates in the ion source[10-12] where $D^+$, $D_2^+$, and $D_3^+$ are accelerated to high energy. A portion of the deuterium gas fed into the ion source leaves as the ion beam. The remainder is forced to flow, through a restrictive 50 cm tall, 15 cm wide, 260 cm long rectangular neutralizer together with the ion beam. In the beamline, the gas is pumped with a total $D_2$ pumping speed of $2 \times 10^6$ l/s on cryopanels lining the two side walls.[13] Charge exchange collisions between beam particles and gas molecules in the neutralizer convert a fraction of the ion beam into neutral particles. Following dissociation of molecular particles, the relationship between the atomic neutral fraction and the neutralizer linear gas density is given by

$$f_0(\pi) = \frac{\sigma_{10}}{\sigma_{10} + \sigma_{01}} \left[ 1 - e^{-(\sigma_{10} + \sigma_{01})\pi} \right] \qquad (1)$$

where $\sigma_{01}$ and $\sigma_{10}$ are the electron loss and capture cross sections, respectively, and $\pi$ is the gas line density.[14] Upon exiting the ion source, the beam is 100% ionic, consisting of $D^+$, $D_2^+$, and $D_3^+$. As it travels down the neutralizer, the composition changes to $D^+$ and $D^0$ with three energy components for each: E, E/2, and E/3. Half- and third-energy particles arise upon dissociation of $D_2^+$ and $D_3^+$, respectively. The maximum neutral fraction occurs under equilibrium ($\pi \rightarrow \infty$)

conditions. Since neutralizers operate with less than equilibrium line densities, changes in $\pi$ produce changes in the neutral power delivered on target.

Upon exiting the neutralizer, the mixed ion and neutral particle beam enters an electromagnet. If energized, the magnet sweeps the charged particles from the beam to the ion dumps. Neutral particles are undeflected and next encounter the beamline calorimeter. For these experiments, the internal beamline calorimeter was always raised, allowing the beam to enter the drift duct and proceed to the target chamber calorimeter. Beam power was measured on this calorimeter via waterflow calorimetry and beam profiles were computed from temperature rises of an array of embedded thermocouples. CENA data were acquired with the magnet energized.

Instrumentation at the test facility provided for the measurement of beam power, beam composition, beam profiles, light emission, and gas pressure. Waterflow calorimetry was used to measure the energy deposited on the full- and half-energy ion dumps, the neutralizer and collimators (in one combined water circuit), and the target chamber calorimeter.[15] Beam composition (i.e., the relative proportions of the extracted $D^+$, $D_2^+$, and $D_3^+$) was determined using a variety of techniques,[8] but for this study results from Doppler-shift spectroscopy of the light emitted by the beam in the neutralizer were used.[16] Beam profiles and divergence angles were derived from least square fits to data from thermocouples embedded in the calorimeter.[17]

### B. Charge Exchange Neutral Analyzer

A CENA with an E ∥ B deflection scheme was one of the techniques used to determine neutral beam composition.[7,8] Here, interest is not in the beam composition, but rather in the time dependence of each neutral specie. Originally developed to determine the energy distribution of neutral particles escaping magnetically confined plasmas, the analyzer was adopted for the direct detection of particles from a neutral beamline. Figure 3 is a schematic cross-sectional view of the device. An equilibrium deuterium gas cell created ions from the incident neutral particles. A D-shaped electromagnet served as a momentum analyzer separating the full-, half-, and third-energy $D^+$. Mass discrimination was carried out by an electric field parallel to the magnetic field. Each deuterium component fell onto a separate Faraday cup allowing concurrent detection.

Collimation in the analyzer determined the analyzer's acceptance. One millimeter holes at either end of a 46 cm long deuterium gas cell, located 14 m

from the ion source, permitted acceptance only of particles emanating from a 6 cm diameter spot on the ion source. This spot was vertically centered on the 12 cm wide by 43 cm tall ion source, but lay entirely on the right-hand side. As a result of the collimation, the acceptance in velocity space was limited to a half-angle of 0.12°. This is to be compared to beamlet 1/e-half-angles of order 0.5° and 1° parallel and perpendicular, respectively, to the grid rails. The acceptance of the analyzer was considerably smaller than the emittance of the ion source.

### C. Other diagnostics

Pressure information was available from three nude Bayard-Alpert ionization gauges. Locations for two of these gauges are indicated in Fig. 2. The third gauge was connected to the target chamber. Time responses of the ion gauge controllers were 2 ms.[18]

During these tests the target chamber was primarily pumped by the cryopanels in the beamline. Gas generated in the target chamber predominantly flowed into the beamline since the ~ 50,000 l/s conductance of the drift duct far exceeded the ~ 2000 l/s speed of the target chamber turbomolecular pump. (Cryopanels in the target chamber were non-functional during these tests.) Due to the high pressures in the drift duct, considerable Balmer series light emission resulted. Information relevant to the time dependence of the beam power was obtained from a photodiode, fiber-optically coupled to the port labelled Duct H-Alpha Monitor in Fig. 2, observing drift duct light emission.[8] The photodiode was sensitive to visible and near-infrared light and had a time response of order 1 ms.

## II. RESULTS

Previous analysis of the TFTR beam's neutral fraction, as measured on the target chamber calorimeter, indicated anomalously low beam neutralization; see Fig. 4.[1] Measured data points lie below the solid line. Values of the neutral fraction for these data points were obtained from waterflow calorimetry on the calorimeter. (Neutral fraction is the ratio of energy delivered to the calorimeter on a shot with the magnet on to that with the magnet off.) Neutralizer line densities of these points were derived from the VSTS calculations. Left to right the five data points correspond to ion source gas supply rates of 13, 15, 17, 19, and 21 torr-l/s. Neutral fractions predicted for an extracted 78% $D^+$, 15% $D_2^+$, 7% $D_3^+$

beam are given by the solid line. Data points to the left of the line are corrections to the prediction due to small variations in ion beam composition with gas throughput. It is obvious that the neutralizer line density is a factor of three less than that predicted by room temperature gas.

Figures 5 and 6 show the time dependence of the full-, half-, and third-energy neutral fluxes (*a*, *b*, *c*, respectively) delivered to the CENA for gas feed rates of 13 and 21 torr-l/s, respectively. The digitizer sample rate was 100 Hz for all data to be shown.

Steady-state levels (i.e., the plateau following the turn-on transient) of the full- and third-energy component signals increased with gas throughput. The steady-state level of the half-energy component behaved differently, decreasing with increasing gas throughput. Both the full- and third-energy component signals exhibited pronounced turn-on transients. Increasing gas throughput decreased the ratio of the transient peak to the steady-state level. Again, the half-energy component behaved differently showing only a modest transient at low throughput, and none for operation above 15 torr–l/s. For the full- and third-energy components which had a turn-on transient, the magnitude of the transient peak increased with gas throughput, becoming independent of gas throughput above 17 torr-l/s.

Table 1 gives the measured exponential decay time of the turn-on transient. Due to the fluctuating nature of the signal, the time was computed as the average of envelopes for the maximum and minimum of the fluctuation. The trend was to faster transients as the throughput decreased. Error bars for this measurement are ± 25%, due to the fluctuations and the 10 ms sample time of the digitizer.

The turn-on transient is also evident in Fig. 7 in the signal of light emission from the drift duct. Part *c* of the figure is the light emission, *b* is the CENA signal for the full-energy component, and *a* is the pressure in the drift duct. Early in the pulse, when the CENA signal peaks, there is insufficient gas in the duct for beam excitation and light emission is low. Only as the duct pressure increases does a transient appear on the light signal. It disappears with the CENA transient. As the throughput of the gas into the ion source is increased, the light emission transient disappears, only being observed at throughputs of 13 and 15 torr-l/s.

It is apparent from Figs. 5 and 6 that the flux of particles for all three components has a pronounced fluctuation. Peak-to-peak oscillations of 20% were observed during this experiment. The apparent frequency of the oscillation, as recorded by the 100 Hz digitizer, is 20 Hz.

## III. DISCUSSION

### A. Vacuum System Transient Simulator

The Vacuum System Transient Simulator (VSTS) computer program was used to model the time dependence of the pressure in the neutralizer.[9] This program follows the viscous, transition, molecular flow evolution as pressure changes both spatially and temporally. The computed time and spatial dependence of the neutralizer pressure provides a prediction for the time evolution of the gas line density. These line densities were taken to be the baseline for the neutralizer operating at room temperature.

When a beam is extracted from an ion source, a fraction of the gas flowing into the source is converted to energetic ions and accelerated away. This diversion of gas effectively decreases the throughput of gas into the ion source, decreasing both the neutralizer and ion source pressures. A new pressure distribution is established in which the ion source pressure and neutralizer line density are lower. This phenomenon is generally referred to as 'beam pump out' and is the cause of the turn-on transients in Figs. 5 and 6. VSTS was used to simulate this effect. For the cases of interest, 60 A of ions were extracted from the ion source. At this current and a beam composition of 78% $D^+$, 15% $D_2^+$, and 7% $D_3^+$,[8] approximately 7 torr-l/s of gas is converted into beam ions.

Ion source, neutralizer, and beamline were all included in the model. The 40 l ion source was connected to the neutralizer via a duct having the 2400 l/s molecular flow conductance of the accelerator grids.[19] To provide information regarding the pressure distribution along the neutralizer, it was modelled as four 65 cm long sections each 15 cm wide by 50 cm tall. A $5x10^4$ l box with a pumping speed of $10^6$ l/s was used to simulate the beamline. Room temperature gas was assumed throughout. VSTS uses a finite difference technique to solve the coupled differential equations.

Results of the VSTS simulation are given in Fig. 8. Shown are the neutralizer line densities as a function of time for the five ion source gas feed rates of interest. Gas throughput is throttled back at 100 ms to simulate beam pump out. For all cases, the approach to steady-state pressure following both the initial and the reduced gas throughputs is approximately exponential, with time constants of order 40 ms. Since the ion source and neutralizer are coupled together, the time constant is a composite of that for the ion source to empty into the neutralizer and for the neutralizer to empty into the beamline. The composite

time constant is essentially that of the neutralizer since the time constant of the smaller ion source is of order 5 ms.

**B. Gas heating**

The anomalously low neutral fractions of Fig. 4 imply a mechanism such as heating of the neutralizer gas by the beam. A theory based on this mechanism has been used to explain the neutralization results of the JET and Fontenay-aux-Roses beamlines.[5] Application of this theory to the present data at 21 torr-l/s requires the assumption of a high neutralizer plasma electron temperature of 20 eV to account for the apparent three-fold decrease in the neutralizer line density. Under these conditions, the gas temperature at the ion source end of the neutralizer is predicted to be 4000 K. For the case of high gas efficiency, i.e., 13 torr-l/s, assumption of a nonphysical electron temperature of 125 eV, with resultant gas temperatures of 5000 K, is necessary to attain agreement with experiment.

At beam turn-on there is a transient, associated with beam pump out, occurring over the time required for the ion source/neutralizer system to reach a new pressure distribution. As indicated in Fig. 8, the time for the system to reach this new equilibrium should be of order 40 ms. This is considerably slower than the time associated with beam heating of the neutralizer gas. The gas heating time is that for a hot gas molecule to traverse one-half the short, 15 cm, dimension of the neutralizer, namely ~ 60 μs.[20] Since this is much shorter than the pump-out time, it is assumed that the gas is rapidly heated and the system then comes to equilibrium at the elevated temperature, and with reduced throughput. Table 1 gives the measured turn-on transient times. Agreement between the measured and predicted widths is good; the predicted 40 ms lies within the range of the measurements.

Evidence presented in Table 1 indicates that the time associated with the turn-on transient decreases as the throughput of gas into the ion source decreases. Such behavior supports a conjecture that gas heating increases as the throughput decreases. It is also observed, from Fig. 4, that equilibrium conditions are approached as more gas is added. At high gas throughput, the neutralizer line density is a factor of three less than anticipated, while at low throughput the discrepancy increases to 4.6. This indicates again that gas heating increases as the throughput decreases. Such scaling is contrary to the theory.[5] Additional theoretical work to develop a model capable of explaining both JET and TFTR data is warranted.

### C. Shot-to-shot steady-state level variation

Relative variations in the steady-state level of the CENA signals as a function of gas throughput were compared with predictions based on the inferred line densities of Fig. 4. (Inferred line densities correspond to the data points to the left of the solid line.) In this analysis a full treatment of the neutralization process,[10] not Eq. (1), is necessary. The variation in the full-energy component signal level with gas throughput can be explained by changes in the neutralization efficiency at the inferred line densities. Data for the third-energy component can be explained by changes in both the line density and the extracted $D_3^+$ fraction. As the ion source gas throughput is varied, the relative fractions of the beam extracted as $D^+$, $D_2^+$, and $D_3^+$ changes. The extracted ion beam composition was determined from analysis of the Doppler-shifted light emission in the neutralizer.[16] Results are given in Fig. 9.[8]

Data for the half-energy component cannot be explained by changes in the neutralizer line density and/or the extracted $D_2^+$ fraction. The effects of decreasing $D_2^+$ fraction and increasing neutralization efficiency with increasing gas throughput are predicted to approximately cancel. Measurements showed that the half-energy CENA signal increased nearly 50% as the throughput was increased from 13 to 21 torr-l/s.

Possible explanations for the observations are an improvement in the half-energy component divergence or a shift of the $D_2^+$ ions into the acceptance of the CENA as the gas throughput increased. The half-energy component beam-averaged divergence, inferred from the width of the Doppler-shifted light, exhibited an approximate 20% increase over the range of gas flows studied. To the extent that the beam-averaged divergence reflects the divergence in the spot viewed by the CENA, the measured change is insufficient to explain the results. Local changes, exceeding beam-averaged changes, in the $D_2^+$ density or divergence within the 6 cm spot on the ion source viewed by the CENA, could be responsible. Since the CENA observes only 5% of the total 516 $cm^2$ extraction area of the ion source, it is a local measurement in both space and angle. It is possible that there are variations in the extracted ion current densities (and hence beam optics) across the ion source, and that these variations are a function of ion source operating pressure. Mapping of both the vertical and horizontal emittance for all components would be required to resolve this question.

Adding gas beyond the 21 torr-l/s of the rightmost point in Fig. 4 can only improve the neutral fraction 4% to the level of the near-equilibrium solid line.

### D. Turn-on Transient

For each pulse, a comparison can be made of the predicted and measured values of the ratio of the peak CENA signal level to the steady-state level (= peaking factor). At beam turn on, the neutralizer line density corresponds to the peak values of Fig. 8. After beam turn on, the line density shifts to the points to the ieft of the solid line in Fig. 4. The peaking factor increases with decreasing gas throughput since the initial peak value corresponds to nearly equilibrium line density, and does not vary much with throughput, while the steady-state level decreases with decreasing throughput. Due to the oscillatory nature of the signals, error bars on the computation of the peaking factor are ± 15%.

Over the range of gas throughputs studied, the full-energy component peaking factor is 15 to 30% higher than that predicted by the inferred change in the neutralizer line density. For the third-energy component, agreement between measurements and predictions is good over the entire range of throughputs studied, if as before, changes in both the line density and beam composition are taken into account.

Turn-on transients are nearly absent from the half-energy component signals. For this component, the improved neutralization efficiency occurring during the turn-on transient should be nearly cancelled by the decrease in the extracted $D_2^+$ component fraction. At high gas throughput, the effect of the $D_2^+$ fraction should dominate the neutralization efficiency, and the turn on should be depressed; the signal should increase by 25% during turn on. Rather than exhibiting this predicted behavior, the data indicate slight peaking. At low throughput the reverse is predicted; neutralization efficiency changes should dominate species changes. Agreement between predictions and measurements is reasonably good at low throughput.

At high throughput there is a discrepancy of order 30% for the full-energy component. Under these conditions the measured full-energy peak is larger than expected, while that for the half-energy component is smaller. Implications are that there are dynamic spatial and/or velocity-space nonuniformities of the type described in the previous section to explain the shot-to-shot behavior of the steady-state level of the half-energy component. Observations suggest that the dynamics are such that the local effects of the $D^+$ and $D_2^+$ are competing; one increasing while the other is decreasing. Beam current and plasma density are constant in

time. It is postulated that ionic species profiles are nonuniform across the ion source and change with time and gas throughput.

Data from the light emission diagnostic supports the fact that there was a turn-on neutral particle flux transient at low gas throughput. As opposed to the CENA, the field-of-view of the photodiode includes most of the beam. Almost all of the beam's phase-space contributes to the signal. Light is emitted by both the beam and the background gas due to excitation in their mutual collisions, but most is Doppler-shifted emission from beam atoms.[8] The amount of Doppler-shifted light emitted is proportional to $n_o n_b$ where $n_o$ and $n_b$ are the background gas and beam densities, respectively.

Figure 7 shows a steady rise in light signal due to the rising gas pressure. Superimposed on this rise is the turn-on transient time shifted to the high pressure side of the CENA transient. As more gas was added to the ion source (on a shot by shot basis), the light emission peak disappeared. This is attributed to the diminishing effect of neutralizer line density as the cause of the transient. At low throughput, the turn-on transient has been attributed to the neutralizer line density changing. The transient is a true power transient, and as a result can be observed in the beam integrated light signal. At high gas throughput, the transient cannot be explained by changes in the neutralizer line density. It has been postulated that the effect is due to plasma in the ion source redistributing itself. The CENA, being highly collimated, is sensitive to such changes, even though the gross properties of the beam do not change. Since the changes do not affect the neutral beam power, they do not appear in the light signal.

Variations in the beam divergence as a function of gas throughput are shown in Table 2. Most curious is the variation of the divergence parallel to the grid rails; no variation in this component of the divergence was expected. Since the algorithm used to compute the divergence assumes beam uniformity at the ion source, uniformity variations could be responsible, further supporting the nonuniformity conjecture.

### E. 720 Hz fluctuation

The apparent 20 Hz fluctuation in the CENA data was actually 720 Hz when observed on an oscilloscope. (Data acquired by the 100 Hz digitizer were aliased to a frequency of 20 Hz.) The source of the 720 Hz was the arc power supply. Ripple on the arc power supply was transferred to the plasma density and then to the extracted beam. A 3% peak-to-peak ripple was observed on the beam current,

implying a 3% peak-to-peak ripple on the beam power, the high voltage accelerating power supply having a well-regulated voltage.

Figure 10 shows a tune of the ion source at a constant accelerating voltage of 95 kV (a value slightly lower than the 100 kV operating point of the present study). A quadratic least squares fit to the data is shown. At the operating perveance (defined as beam current/beam voltage$^{1.5}$) of $1.95 \times 10^{-6}$ $AV^{-1.5}$, a change of 3% in perveance corresponds to a 10% change in divergence perpendicular to the grid rails.

Beam profiles are generally modelled with the assumption of a gaussian angular distribution function

$$f(\theta) = \frac{\exp\left[-\left(\theta/\theta_e\right)^2\right]}{\theta_e \sqrt{\pi}} \qquad (2)$$

for each data point on the ion source;[21] $\theta_e$ is the beam divergence. Since the CENA is highly collimated, it accepts only a small fraction of possible angles. The distribution function for those particles collected by the CENA (i.e., those with $\theta \sim 0$) is inversely proportional to $\theta_e$. Fluctuations on the order of those on the divergence are, therefore, expected on the CENA signals.

Fluctuations of the beam power density (all points on the ion source contributing) are smaller than those on the CENA signals. Generalizing the power density expression[21] to a rectangular ion source with bi-gaussian divergence, one finds that the central power density at a location z downstream from the ion source is

$$P(x=0, y=0) = \frac{P_0}{4 x_0 y_0} \operatorname{erf}\left(\frac{x_0}{z \tan\theta_x}\right) \operatorname{erf}\left(\frac{y_0}{z \tan\theta_y}\right) \qquad (3)$$

where $P_0$ is the total beam power, $x_0$ and $y_0$ are the ion source half-dimensions in the x and y directions, $\theta_x$ and $\theta_y$ are the 1/e-divergences in the x and y directions, and erf is the error function. For typical TFTR neutral beam operating conditions (i.e., $x_0 = 6$ cm, $y_0 = 21.5$ cm, $\theta_x = 0.4°$, $\theta_y = 1°$, and $z = 12.75$ m), a 10% peak-to-peak variation in $\theta_y$ produces a 5% peak-to-peak variation in the central beam power

density at the plasma. Ripple on the arc power supply translates into fluctuations in both the amplitude ($P_0$) and shape ($\theta_x$, $\theta_y$) of the beam.

Figure 11 shows the limits of the predicted vertical profiles of the beam for the fluctuation; $\theta_y$ values of 0.95° and 1.05° were used. The lines correspond to the beam profiles at the peaks and valleys of the fluctuation. The adjustment of the beam spatial profile to the beam current ripple depends on where the beam is operating on its tuning curve. Figure 11 is for a case of underdense operation, that is, perveance is to the left of the minimum in Fig. 10. Under such conditions, excursions of increasing beam current cause the central power density to increase due to both improving beam optics and increasing beam current. The 5% power density increase (peak to peak) associated with the optics and the 3% increase of the beam current add, resulting in an 8% peak-to-peak power density excursion. For the case of overdense operation, that is, perveance to the right of the minimum in Fig. 10, there is only a 2% central power density excursion since the two effects subtract. In this case, the effect is pronounced in the wings of the profile. Operation 'on perveance' (i.e., at the tuning curve minimum) is ideal, exhibiting minimal beam profile excursions due to power supply ripple. Due to the parabolic nature of the tuning curve, the farther the operating point is from the minimum, the greater the change in the divergence for a given perveance fluctuation.

## ACKNOWLEDGMENTS

We wish to acknowledge technical contributions from M. Cropper, J. Edwards, V. Garzotto, J. Desandro, G. Johnson, B. McCormack, F. Polom, R. Shoemaker, J. Thomas, R. Yager, the TFTR Neutral Beam Operations Staff, and the TFTR computer division. This work was supported by the U.S. DOE under contract No. DE-AC02-76-CHO-30[illegible].

## REFERENCES

[1]J. H. Kamperschroer, G. M. Gammel, H. W. Kugel, L. R. Grisham, T. N. Stevenson, A. von Halle, M. D. Williams, and T. T. C. Jones, J. Vac. Sci. Technol. A **7**, 83 (1989).

[2]M. Fumelli, P. Bayetti, R. Becherer, F. Bottiglioni, M. Desmons, P. Raimbault, F. P. G. Valckx, in *Proceedings of the Thirteenth Symposium on Fusion Technology*, Varese, Italy, 1984 (Pergamon, Oxford, 1984), Vol. 1, p. 617.

[3]P. Bayetti, F. Bottiglioni, G. Martin, and J. Paméla, Rev. Sci. Instrum. **57**, 62 (1986).

[4]H. D. Falter, R. S. Hemsworth, G. H. Deschamps, A. P. H. Goede, T. T. C. Jones, P. Massmann, M. J. Mead, and A. Stäbler, in *Proceedings of the Eleventh Symposium on Fusion Engineering*, Austin, 1985 (IEEE, New York, 1986), Vol. 2, p. 786.

[5]J. Paméla, Rev. Sci. Instrum. **57**, 1066 (1986).

[6]J. Kim, General Atomics, private communication.

[7]A. L. Roquemore, G. Gammel, G. W. Hammett, R. Kaita, and S. S. Medley, Rev. Sci. Instrum. **56**, 1120 (1985).

[8]H. W. Kugel, G. M. Gammel, L. R. Grisham, R. Kaita, J. H. Kamperschroer, R. A. Langley, C. W. Magee, S. S. Medley, T. J. Murphy, A. L. Roquemore, and M. D. Williams, Rev. Sci. Instrum. **60**, 37 (1989).

[9]The Vacuum System Transient Simulator was written by J. Sredniawski, of Grumman Aerospace Co., Bethpage, NY, as an aid in the design of the TFTR vacuum system.

[10]P. A. Pincosy, K. W. Ehlers, A. F. Lietzke, H. M. Owren, J. A. Paterson, R.V. Pyle, and M. C. Vella, Rev. Sci. Instrum. **57**, 2705 (1986).

[11]P. D. Weber, H. M. Owren, J. A. Paterson, P. A. Pincosy, R. V. Pyle, R. P. Wells, and M. C. Vella, Rev. Sci. Instrum. **57**, 2714 (1986).

[12]M. C. Vella, W. S. Cooper, P. A. Pincosy, R. V. Pyle, P. D. Weber, and R. P. Wells, Rev. Sci. Instrum. **59**, 2357 (1988).

[13]L. C. Pittenger, R. R. Stone, L. E. Valby, and L. R. Pedrotti, in *Proceedings of the Seventh Symposium on the Engineering Problems of Fusion Research*, Knoxville, 1977 (IEEE, NY, 1977), Vol. 1, p. 555.

[14]For a complete treatment of beam neutralization see K. H. Berkner, R. V. Pyle, and J. W. Stearns, Nucl. Fusion **15**, 249 (1975), or J. Kim and H. H. Haselton, J. Appl. Phys. **50**, 3802 (1979).

[15]J. H. Kamperschroer, L. R. Grisham, L. E. Dudek, G. M. Gammel, G. A. Johnson, H. W. Kugel, L. Lagin, T. E. O'Connor, P. A. Shah, P. Sichta, T. N. Stevenson, A. von Halle, M. D. Williams, and R. Bastasz, Rev. Sci. Instrum. (to be published).

[16]J. H. Kamperschroer, H. W. Kugel, M. A. Reale, S. L. Hayes, G. A. Johnson, J. L. Lowrance, P. A. Shah, P. Sichta, B. W. Sleaford, M. D. Williams, and P. M. Zucchino, Rev. Sci. Instrum. **58**, 1362 (1987).

[17]V. Elisher, V. Jacobson, and E. Theil, in *Proceedings of the Ninth Symposium on Engineering Problems of Fusion Research*, Chicago, 1981 (IEEE, New York, 1981), Vol. 1, p. 941.

[18]Granville-Phillips, Co., Boulder, CO.

[19]J. E. Willis and K. H. Berkner, in *Proceedings of the Ninth Symposium on Engineering Problems of Fusion Research*, Chicago, 1981 (IEEE, New York, 1981), Vol. 1, p. 798.

[20]J. Paméla, "Gas Heating Effects in the Neutralizers of Neutral Beam Injection Lines," Euratom Report EUR-CEA-FC-1279, Oct. 1985.

[21]J. Kim and J. H. Whealton, Nucl. Instrum. & Methods **141**, 187 (1977).

**Table 1.** Time Constants of the Turn-on Transients for the Three Neutral Beam Constituents.

| gas throughput | full-energy | half-energy | third-energy |
|---|---|---|---|
| 13 torr-l/s | 28 ms | -- | 24 ms |
| 15 | 38 | 40 ms | 36 |
| 17 | 40 | -- | 38 |
| 19 | 47 | -- | 38 |
| 21 | 52 | -- | 49 |

**Table 2.** Beam Divergences Parallel and Perpendicular to the Grid Rails as a Function of Gas Throughput.

| gas throughput | beam current | beam voltage | perveance | parallel divergence | perpendicular divergence |
|---|---|---|---|---|---|
| 13 torr-l/s | 61 A | 100 kV | $1.929 \times 10^{-6}$ AV$^{-1.5}$ | 0.53° | 0.91° |
| 15 | 61.7 | 100 | $1.951 \times 10^{-6}$ | 0.50 | 0.88 |
| 17 | 60 | 100 | $1.897 \times 10^{-6}$ | 0.47 | 0.75 |
| 19 | 61.6 | 100 | $1.948 \times 10^{-6}$ | 0.47 | 0.87 |
| 21 | 61.6 | 100 | $1.948 \times 10^{-6}$ | 0.44 | 0.87 |

**Figure Captions**

Figure 1. Schematic plan view of TFTR Neutral Beam Test Facility.

Figure 2. Schematic elevation view of TFTR Neutral Beam Test Facility.

Figure 3. Schematic cross-sectional view of the Charge Exchange Neutral Analyzer (CENA).

Figure 4. Neutral power fraction versus neutralizer line density. Solid line is a prediction based on room temperature gas and a beam composed of 78% $D^+$, 15% $D_2^+$, and 7% $D_3^+$. Points below the line are the measured data points. Points to the left of the line are predictions with actual beam composition.

Figure 5. CENA data at a gas throughput of 13 torr-l/s into the ion source; a), b), and c) are the full-, half-, and third-energy components, respectively.

Figure 6. CENA data at a gas throughput of 21 torr-l/s into the ion source; a), b), and c) are the full-, half-, and third-energy components, respectively.

Figure 7. Signals from: a) ion gauge in the drift duct, b) full-energy component from the CENA, and c) light emission from the drift duct, all for the case of 13 torr-l/s.

Figure 8. Time dependence of the neutralizer line density, predicted by the Vacuum System Transient Simulator, as a function of gas throughput into the ion source. Lines a), b), c), d), and e) are for gas throughputs into the ion source of 21, 19, 17, 15, and 13 torr-l/s, respectively.

Figure 9. Extracted beam composition as a function of gas throughput into the ion source.

Figure 10. An ion source tune performed at a fixed extraction voltage of 95 kV. The divergence is the 1/e angular half-width measured perpendicular to the grid rails using a fit to an array of thermocouples on the calorimeter. A parabolic fit to the data points is shown.

Figure 11. Typical neutral beam vertical power density profiles, at the location of the TFTR plasma, in the crests and valleys of the 720 Hz fluctuation. Divergences are 0.95° (solid line) and 1.05° (dashed line).

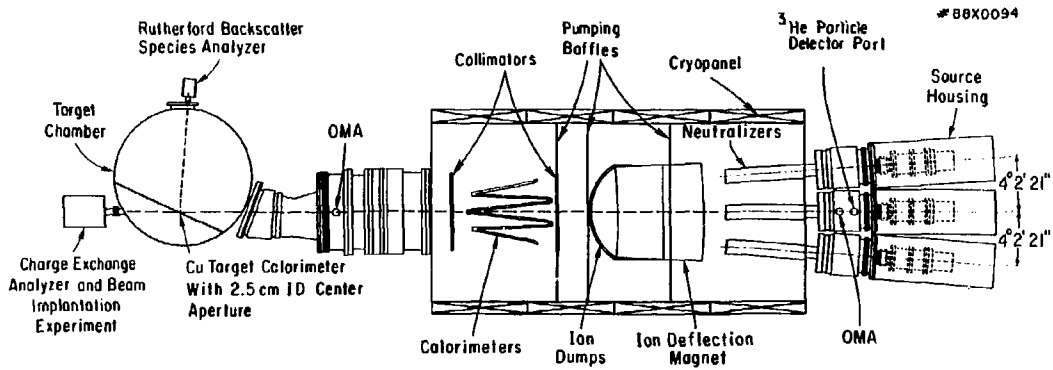
#88X0094
Rutherford Backscatter
Species Analyzer
Target
Chamber
OMA
Collimators
Pumping
Baffles
Cryopanel
$^3$He Particle
Detector Port
Source
Housing
Neutralizers
4°
2'
21"
4°
2'
21"
Charge Exchange
Analyzer and Beam
Implantation
Experiment
Cu Target Calorimeter
With 2.5 cm ID Center
Aperture
Calorimeters
Ion
Dumps
Ion Deflection
Magnet
OMA

Fig. 1

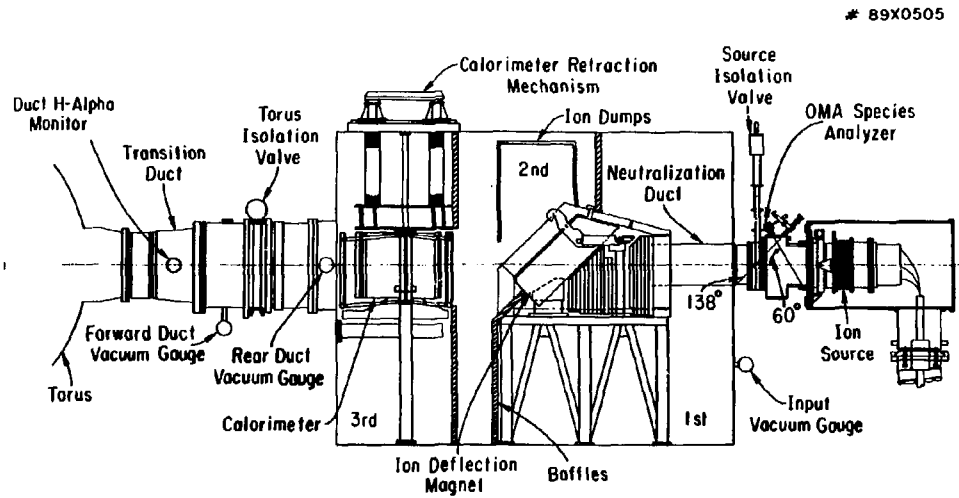
# 89X0505
Calorimeter Retraction Mechanism
Source Isolation Valve
Duct H-Alpha Monitor
Torus Isolation Valve
Ion Dumps
OMA Species Analyzer
Transition Duct
2nd
Neutralization Duct
138°
60°
Forward Duct Vacuum Gauge
Rear Duct Vacuum Gauge
Ion Source
Torus
Calorimeter
3rd
1st
Input Vacuum Gauge
Ion Deflection Magnet
Baffles

Fig. 2

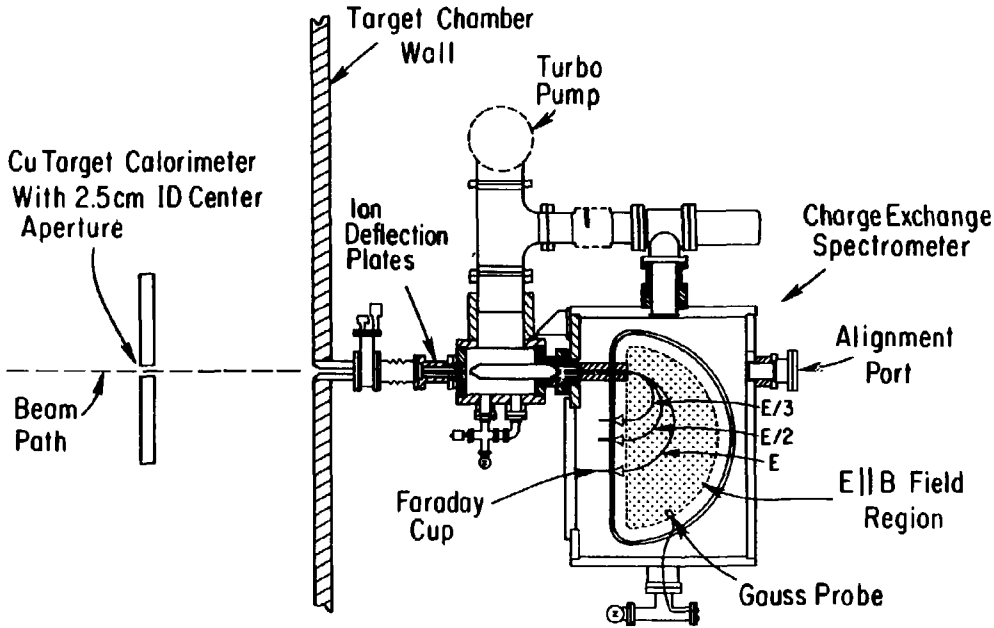
Target Chamber
Wall
Turbo
Pump
Cu Target Calorimeter
With 2.5cm ID Center
Aperture
Ion
Deflection
Plates
Charge Exchange
Spectrometer
Alignment
Port
Beam
Path
E/3
E/2
E
E||B Field
Region
Faraday
Cup
Gouss Probe

Fig. 3

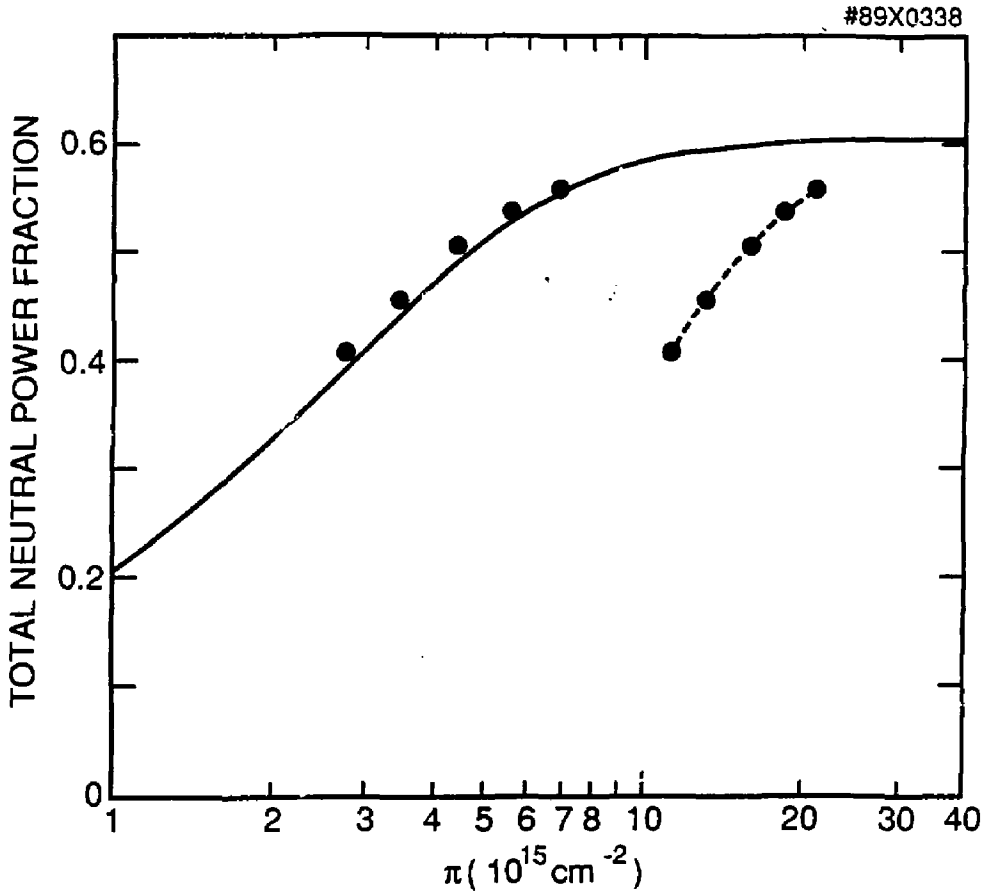
#89X0338
TOTAL NEUTRAL POWER FRACTION
0.6
0.4
0.2
0
1
2
3
4
5
6
7
8
10
20
30
40
π( 10^15 cm^-2 )

Fig. 4

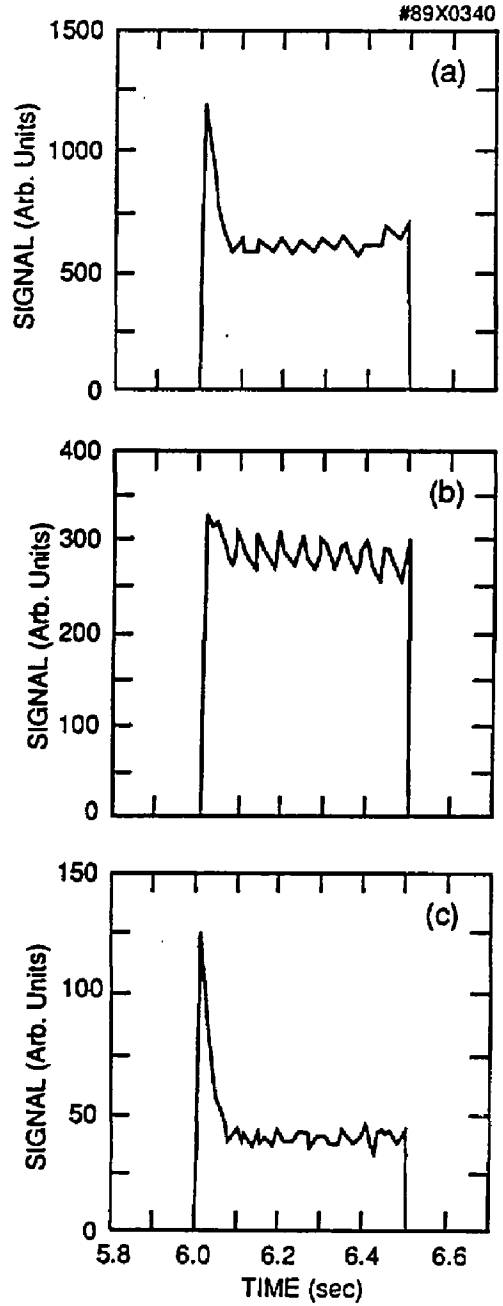
#89X0340
(a)
(b)
(c)
SIGNAL (Arb. Units)
1500
1000
500
0
400
300
200
100
150
50
5.8
6.0
6.2
6.4
6.6
TIME (sec)

Fig. 5

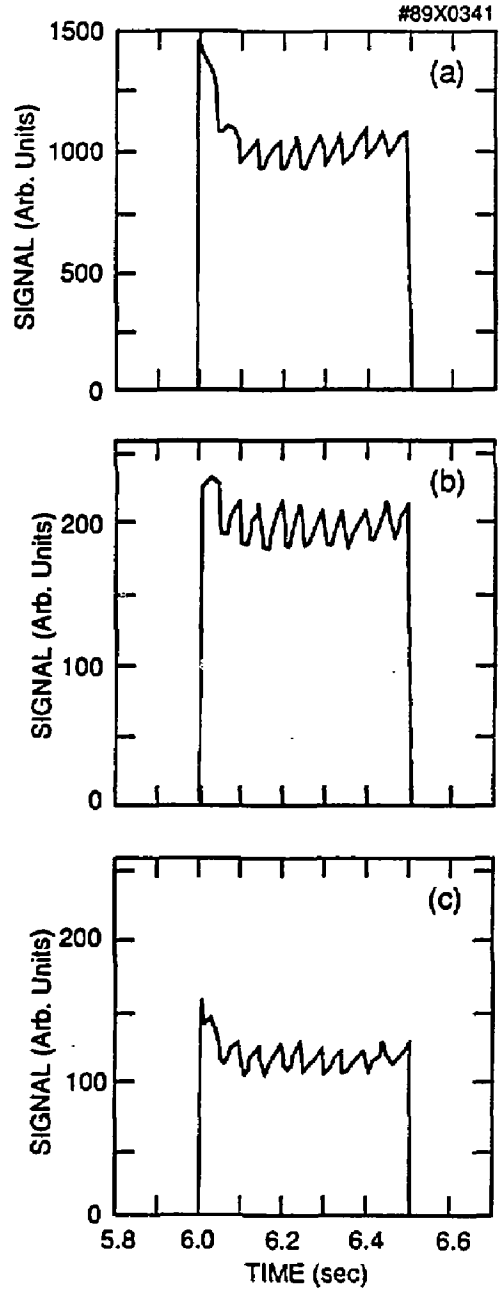
#89X0341
1500
1000
500
0
SIGNAL (Arb. Units)
(a)
200
100
0
SIGNAL (Arb. Units)
(b)
200
100
0
SIGNAL (Arb. Units)
(c)
5.8
6.0
6.2
6.4
6.6
TIME (sec)

Fig. 6

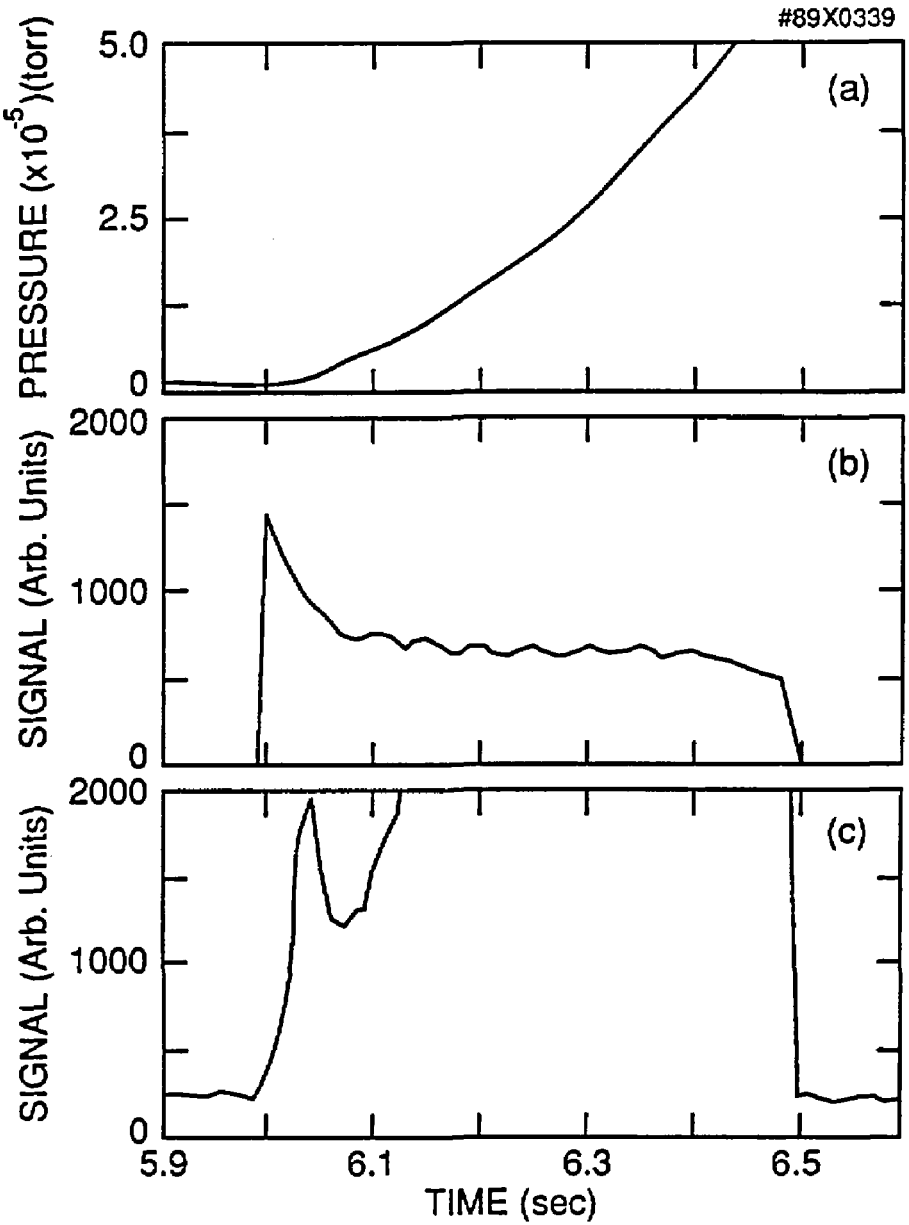
#89X0339
PRESSURE (x10$^{-5}$)(torr)
5.0
2.5
0
(a)
SIGNAL (Arb. Units)
2000
1000
0
(b)
SIGNAL (Arb. Units)
2000
1000
0
(c)
5.9
6.1
6.3
6.5
TIME (sec)

Fig. 7

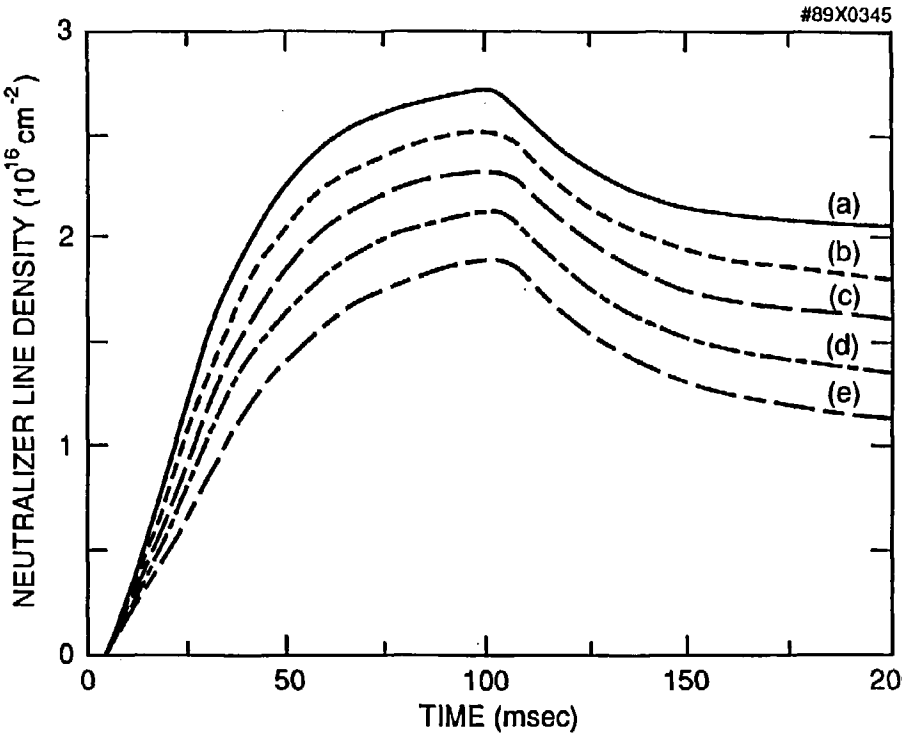
#89X0345
NEUTRALIZER LINE DENSITY ($10^{16}$ cm$^{-2}$)
TIME (msec)
0
1
2
3
0
50
100
150
200
(a)
(b)
(c)
(d)
(e)

Fig. 8

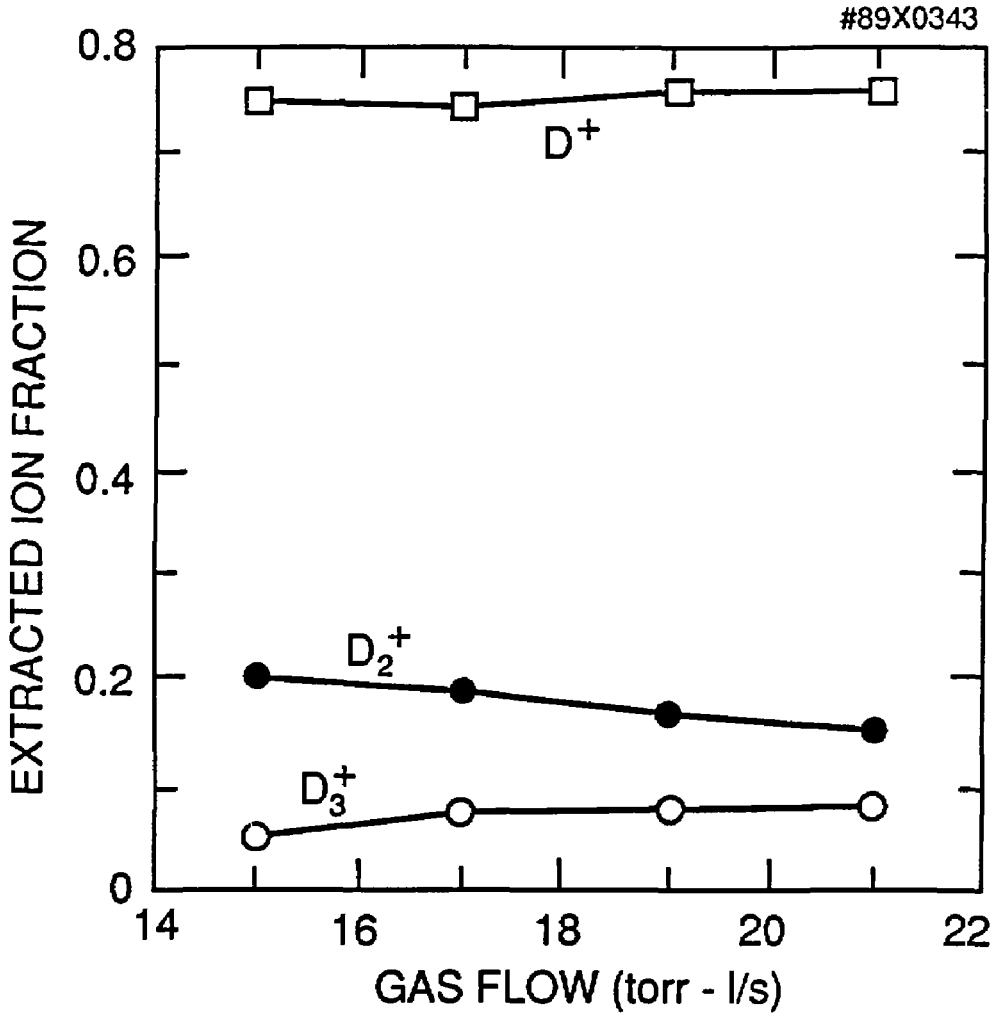
#89X0343
0.8
0.6
0.4
0.2
0
EXTRACTED ION FRACTION
D+
D2+
D3+
14
16
18
20
22
GAS FLOW (torr - l/s)

Fig. 9

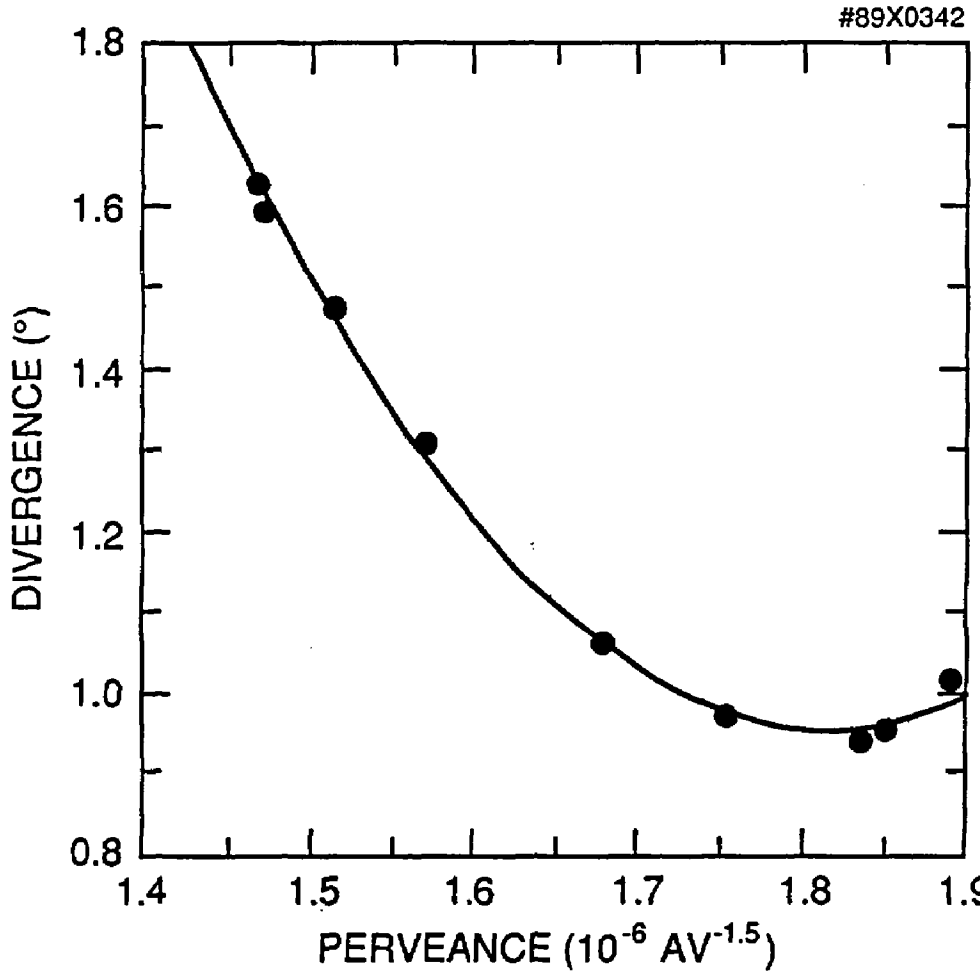
#89X0342
1.8
1.6
1.4
1.2
1.0
0.8
DIVERGENCE (°)
1.4
1.5
1.6
1.7
1.8
1.9
PERVEANCE ($10^{-6}$ $AV^{-1.5}$)

Fig. 10

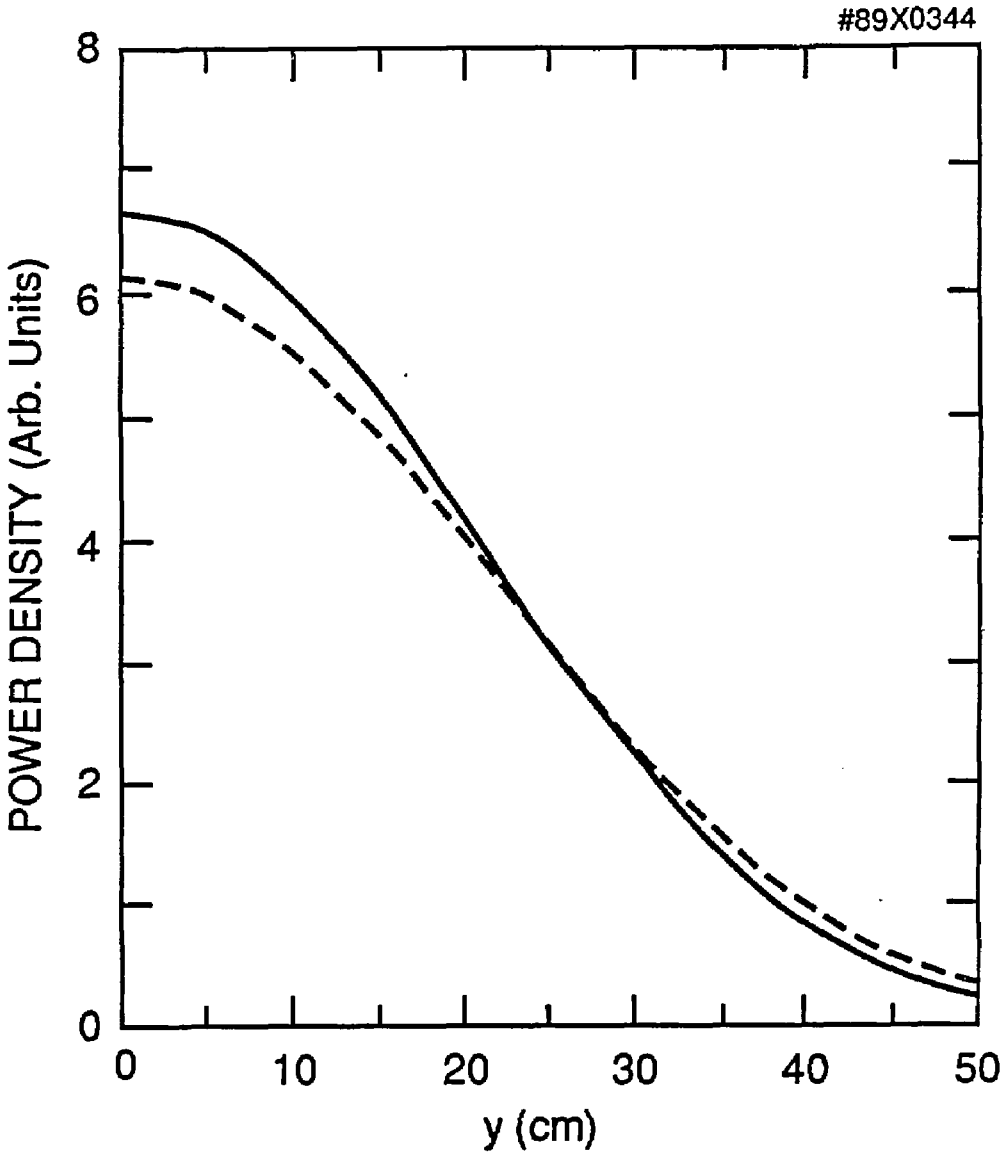


Fig. 11

EXTERNAL DISTRIBUTION IN ADDITION TO UC-420

Dr. Frank J. Paoloni, Univ of Wollongong, AUSTRALIA
Prof. M.H. Brennan, Univ Sydney, AUSTRALIA
Plasma Research Lab., Australian Nat. Univ., AUSTRALIA
Prof. I.R. Jones, Flinders Univ., AUSTRALIA
Prof. F. Cap, Inst Theo Phys, AUSTRIA
Prof. M. Heindler, Institut für Theoretische Physik, AUSTRIA
M. Goossens, Astronomisch Instituut, BELGIUM
Ecole Royale Militaire, Lab de Phys Plasmas, BELGIUM
Commission-European, Dg-XII Fusion Prog, BELGIUM
Prof. R. Boucique, *Rijksuniversiteit Gent*, BELGIUM
Dr. P.H. Sakanaka, Instituto Fisica, BRAZIL
Instituto De Pesquisas Espaciasi-INPE, BRAZIL
Documents Office, Atomic Energy of Canada Limited, CANADA
Dr. M.P. Bachynski, MPB Technologies, Inc., CANADA
Dr. H.M. Skarsgard, University of Saskatchewan, CANADA
Dr. H. Barnard, University of British Columbia, CANADA
Prof. I. Teichmann, Univ. of Montreal, CANADA
Prof. S.R. Sreenivasan, University of Calgary, CANADA
Prof. Tudor W. Johnston, INRS-Energie, CANADA
Dr. Bolton, Centre canadien de fusion magnetique, CANADA
Dr. C.R. James, Univ. of Alberta, CANADA
Dr. Peter Lukac, Komenskeho Univ, CZECHOSLOVAKIA
*The Librarian*, Culham Laboratory, ENGLAND
The Librarian, Rutherford Appleton Laboratory, ENGLAND
Mrs. S.A. Hutchinson, JET Library, ENGLAND
C. Mouttet, Lab. de Physique des Milieux Ionises, FRANCE
J. Radet, CEN/CADARACHE - Bat 506, FRANCE
Ms. C. Rinni, Librarian, Univ. of Ioannina, GREECE
Dr. Tom Mual, Academy Bibliographic Ser., HONG KONG
Preprint Library, Hungarian Academy of Sciences, HUNGARY
Dr. B. *Das Gupta, Saha Inst of Nucl. Phys.*, INDIA
Dr. P. Kaw, Institute for Plasma Research, INDIA
Dr. Philip Rosenau, Israel Inst. of Tech, ISRAEL
Librarian, Int'l Ctr Theo Phys, ITALY
Prof. G. Rostagni, Istituto Gas Ionizzati Del CNR, ITALY
Miss Clelia De Palo, Assoc EURATOM-ENEA, ITALY
Dr. G. Grosso, Istituto di Fisica del Plasma, ITALY
Dr. H. Yamato, Toshiba Res & Dev, JAPAN
Prof. I. Kawakami, Atomic Energy Res. Institute, JAPAN
Prof. Kyoji Nishikawa, Univ of Hiroshima, JAPAN
Director, Dept. Large Tokamak Res. JAERI, JAPAN
Prof. Satoshi Itoh, Kyushu University, JAPAN
*Research Info Center, Nagoya University*, JAPAN
Prof. S. Tanaka, Kyoto University, JAPAN
Library, Kyoto University, JAPAN
Prof. Nobuyuki Inoue, University of Tokyo, JAPAN
S. Mori, JAERI, JAPAN
H. Jeong, Librarian, Korea Advanced Energy Res Inst, KOREA
Prof. D.I. Choi, The Korea Adv. Inst of Sci & Tech, KOREA
Prof. B.S. Liley, University of Waikato, NEW ZEALAND
Institute of Plasma Physics, PEOPLE'S REPUBLIC OF CHINA
Librarian, Institute of Phys., PEOPLE'S REPUBLIC OF CHINA
Library, Tsing Hua University, PEOPLE'S REPUBLIC OF CHINA
Z. Li, Southwest Inst. Physics, PEOPLE'S REPUBLIC OF CHINA
Prof. J.A.C. Cabral, Inst Superior Tecnico, PORTUGAL
*Dr. Octavian Petrus, AL I CUZA University*, ROMANIA
Dr. Jam de Villiers, Fusion Studies, AEC, SO AFRICA
Prof. H.A. Hellberg, University of Natal, SO AFRICA
C.I.E.M.A.T., Fusion Div. Library, SPAIN
Dr. Lennart Stenflo, University of UMEA, SWEDEN
Library, Royal Institute of Tech, SWEDEN
Prof. Hans Wilhelmson, Chalmers Univ of Tech, SWEDEN
Centre Phys des Plasmas, Ecole Polytech Fed, SWITZERLAND
*Bibliotheek, Fom-Inst Voor Plasma-Fysica, THE NETHERLANDS*
Metin Durgut, Middle East Technical University, TURKEY
Dr. D.D. Ryutov, Siberian Acad Sci, USSR
Dr. G.A. Eliseev, Kurchatov Institute, USSR
Dr. V.A. Glukhikh, Inst Electrophysical Apparatus, USSR
Prof. O.S. Pavlichenko, Inst. of Phys. & Tech. USSR
Dr. L.M. Kovrizhnykh, Institute of Gen. Physics, USSR
Nuclear Res. Establishment, Julich Ltd., W. GERMANY
Bibliothek, Inst. Fur Plasmaforschung, W. GERMANY
Dr. K. Schindler, Ruhr-Universitat Bochum, W. GERMANY
ASDEX Reading Rm, c/o Wagner, IPP/Max-Planck, W. GERMANY
Librarian, Max-Planck Institut, W. GERMANY
Prof. R.K. Janev, Inst of Phys, YUGOSLAVIA